Diffraction waves on general two-legged rectangular floating breakwaters

Esmaeel Masoudi[a,*], Lian Gan[a]

[a] *Department of Engineering, Durham University, United Kingdom*

Abstract

In this paper, hydrodynamic characteristics of general two-dimensional rectangular floating breakwaters (FBs) with two legs in water of finite depth and infinite domain subjected to sinusoidal waves are studied using a numerical panel method. A parametric study is carried out in order to quantify the effect of the leg size and the leg angle on diffraction problem, especially on the transmission and reflection coefficients. Results show that legs play an effective role in breakwater's response to incident waves and two-legged FBs could be used for achieving higher efficiencies compared to conventional rectangular FBs. The angle parameter shows that the inverse T-type FB is the best and the Π type FB is the least good in terms of transmission coefficients. However, practical considerations might also be considered when choosing the best FB configuration for different applications.

1. Introduction

Fixed breakwaters for many years have been used to protect shores and increase the use of locations exposed to wave attack for different purposes such as loading and unloading of cargo vessels, fishing and fishing cages, military operations and most recently recreational and touristic facilities. For multiple reasons, including high cost, seabed sedimentation and negative impact on shore ecology, floating breakwaters (FBs) were introduced during last decades as an alternative to fixed breakwaters. FB usually consists of a floating pontoon with finite draft which can suppress waves without causing hindrance to water flux. The movement of FB can be described by three degrees of freedom viz sway, heave and roll.

To obtain the hydrodynamic coefficients, wave forces and moments, and reflection and transmission coefficients of floating structures, various numerical, analytical and experimental approaches have been used. Analytically, Ursell (1949) studied the problem of long horizontal circular cylinder oscillating with small amplitude in water of infinite depth. They deduced wave amplitude as a function of distance from the cylinder and added mass due to the fluid motion. MacCamy and Fuchs (1954) used an eigen-function expansion method to analyze water waves interaction to cylindrical piles and derived wave exciting forces and moments on them. Garrison (1984) employed a Green's function procedure to compute the oblique wave interaction with a cylinder of arbitrary section on the free surface in water of infinite depth. They presented added mass and damping coefficients for rectangular and semi-circular cylinders and found this procedure being accurate and efficient. Lee (1995) studied heave radiation problem of a rectangular body and realized that the non-homogeneous boundary value problem can be linearly decomposed into a homogeneous one. They stated that smaller structure submergence and larger structure width would result in larger wave, added mass and damping coefficients. Abul-Azm and Gesraha (2000) applied an eigen-function expansion method to analyze a moored FB in oblique waves. They noticed that the hydrodynamic behaviour of a pontoon type FB in waves has a strong dependence on the rela-

*Corresponding author

Email addresses: esmaeel.masoudi@durham.ac.uk (Esmaeel Masoudi), lian.gan@durham.ac.uk (Lian Gan)

tive dimension of the cross section, while dynamic properties mostly rely on the inertial characteristics of the structure. Zheng et al. (2004) and Shen et al. (2005) derived an analytical solution for radiation and diffraction problem of a rectangular buoy and presented extensive results for added mass and damping coefficients as well as the effect of bottom sill. Xu et al. (2019) studied wave diffraction problem of a two-dimensional moonpool using domain decomposition scheme and the method of eigen-function expansion. They deduced wave exciting forces, free surface and internal wave elevations and concluded that decreasing density ratio has little effects on the sloshing mode resonance frequencies but can somehow suppress the horizontal wave exciting forces and surface wave elevations. He et al. (2019) analyzed hydrodynamics of an oscillating water column (OWC) by means of an analytical model based on linear wave theory and matched eigen-function expansion method. They introduced a two-level practical optimization strategy on power take off (PTO) damping and proved that this strategy yields similar wave power extraction and wave transmission as the ideal optimization approach. Masoudi and Gan (2020) applied both analytical and numerical methods based on linear wave theory and considered both vertical and horizontal flat submerged breakwaters. They demonstrated that horizontal flat breakwater shows high reflection coefficients over large ranges of incident wave frequencies and could be used as an alternative to conventional FBs.

In the framework of numerical methods , many studies concerned FEM and BEM. As examples, Bai (1975) presented a FEM-based numerical method for solving diffraction problem for oblique plane waves incident upon an infinitely long fixed cylinder on the free surface. Yamamoto et al. (1980) used BEM to solve a two-dimensional problem of the response of the moored floating objects in water waves. They solved the boundary value problem by a potential flow function. Lau et al. (1990) solved a three-dimensional problem of the dynamics of a moored floating object with an arbitrary cross section under the action of regular waves by use of the finite-infinite element method. They derived satisfactory results comparing to analytical solutions even though the meshes used, had been rather coarse. Wu and Taylor (1995) studied the two-dimensional nonlinear time domain free surface flow problem using time marching BEM and FEM approach. They concluded that in many cases the FEM may be more efficient than BEM in terms of the cost of the simulation, but for complex geometries BEM might be a better option. Hur and Mizutani (2003) developed a volume of fluid (VOF) method to estimate the wave forces acting on a three-dimensional submerged breakwater. They explained that their model reproduces the wave forces for both non-breaking and breaking wave conditions without empirical coefficients being used. Michailides and Angelides (2012) studied flexible floating breakwater (FFB), which consists of flexible modules connected with flexible connectors and linear PTO, in longitudinal and transverse directions under the action of linear waves. They deduced that the wave angle, PTO angle and total number of the FFBs' modules could change the produced power dramatically. Chen et al. (2016) built their FEM based on Navier-Stokes equation and VOF method to study the wave energy extraction by two-dimensional oscillating cylinders in linear waves for incompressible viscous flows. Based on wave climate off China's shore and building cost, they suggested that the cylinder diameter must be twice the incident wave height in order to obtain the best energy harvest efficiency. Zhang et al. (2018) carried out a hydrodynamic analysis of a new L-type FB considering linear wave interactions using a $k-\epsilon$ model. They described that this L-type breakwater possesses better wave dissipation ability comparing to Π type FBs under the same plate length. Liu et al. (2019) adopted a lumped mass approach coupled with smoothed particle hydrodynamics (SPH) to study a rectangular FB equipped with protruding plates. They showed that the winged FB has larger reflection and dissipation coefficients than the non-winged one, showing a great improvement for box-type FBs. Masoudi (2019) employed BEM to study inverse T-type FB's hydrodynamic behaviour in linear waves. They concluded that inverse T-type FBs have higher reflection coefficient comparing to rectangular FBs over a wide range of wave numbers. Deng et al. (2019a) studied a novel OWC breakwater with horizontal bottom plate numerically with OpenFoam package and compared it to their experimental results. They concluded that lengthening the bottom-plate can effectively increase the energy dissipation and then lead to lower reflection and transmission coefficients.

Previously in studies such as Gesraha (2006), Günaydın and Kabdaşlı (2007), Zhan et al. (2017) and Masoudi (2019), two types of rectangular FBs, so called the Π type and the inverse T type, were studied using numerical or analytical methods. In fact, these FBs could be characterized by a more general two-legged FB configuration, which is equipped with two external legs that could be made by adding simple columns of steel to conventional rectangular cross section breakwaters. They could be good substitutes for other conventional types of breakwaters with similar effectiveness but using much less materials. In this study, FBs of rectangular cross section with simple rectangular legs are studied numerically in water of finite depth and infinite extent, subject to regular sinusoidal waves. After verification of the numerical model with previous analytical studies, diffraction problem is solved to derive the hydrodynamic characteristics including exciting forces as well as reflection and transmission coefficients. In particular, a parametric study on the expanding angle and the size of the legs are carried out. Also a comparison of transmission coefficients is made and the most efficient configuration is found. Maximum diffraction wave amplitudes in a wide range of incident wave frequencies are also discussed in comparison with conventional breakwaters.

In this study we pay our attention to regular waves only. Mooring system is not considered. It should be noted that for any higher order regular or irregular waves, the hydrodynamic behaviour and parameters may be different.

2. Method

For FBs having large length to the wavelength ratios, fluid can be assumed to be incompressible, inviscid and irrotational. It should be noted that for very large offshore/shore platforms, in which Reynolds number is high, the viscosity effect can be neglected compared to the inertial effect and so the fluid can be assumed irrotational (Gesraha (2006); Deng et al. (2019b); Ghafari and Dardel (2018); Wang et al. (2020)). Furthermore, boundary layer behaviour, hence its separation, is not the main interest in this study. As such, there would be a scalar function called the velocity potential ϕ that satisfies the Laplace equation as shown in Equation (1). The velocity components and pressure then can be expressed by Equation (2) and (3), respectively.

$$\nabla^2 \phi = 0 \tag{1}$$

$$\frac{\partial \phi}{\partial x} = u, \qquad \frac{\partial \phi}{\partial y} = v, \qquad \frac{\partial \phi}{\partial z} = w \tag{2}$$

$$\nabla(\frac{\partial \phi}{\partial t} + \frac{1}{2}\nabla\phi.\nabla\phi + gz + \frac{P}{\rho}) = 0, \tag{3}$$

where u, v and w are velocity components in x, y and z direction respectively. P is the dynamic pressure, ρ is water density, g is the gravitational acceleration and $F(t)$. Basic problem configuration of the breakwater and the coordinate system are defined in Figure 1. It is assumed that a linear wave with amplitude A_i and angular frequency $\omega = 2\pi/T_i$, in which T_i is incident wave period, propagates in a direction at an angle θ to the $+x$ axis. The total potential ϕ_t is composed of incident wave potential ϕ_i, diffraction potential ϕ_d, and radiation potentials ϕ_r. The incident wave potential for a regular sinusoidal wave can be written as $\phi_i = \varphi_i(x,z)\exp(jky\sin\theta)$, in which:

$$\varphi_i = -\frac{jgA_i}{\omega}\frac{\cosh[k(z+h)]}{\cosh(kh)} \exp(jkx\cos\theta), \tag{4}$$

where k is the wave number, j is unit imaginary number and h is the depth of water. Also

$$\omega^2 = gk\tanh(kh), \tag{5}$$

is known as the *dispersion equation*. The diffraction potential ϕ_d is induced by the interaction of incident wave and the breakwater. The induced potential from the motion of structure in three degrees of freedom is known as radiation potential ϕ_r.

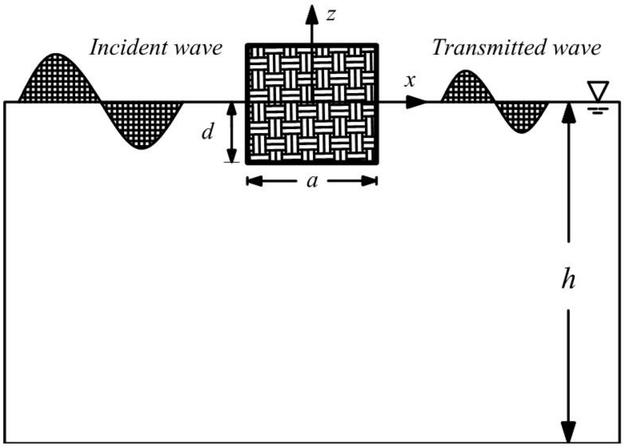

Figure 1: Problem configuration and coordinate system for a two-dimensional rectangular FB.

Referring to Figure 1, the problem is considered as two-dimensional. That is, motions are restricted in heave, sway and roll, denoted as indices 1, 2 and 3, respectively. Hence the total potential ϕ_t could be expressed as:

$$\phi_t = \phi_i + \phi_d + \sum_{L=1}^{3} \phi_r^L \tag{6}$$

where L refers to the assigned motion number and ϕ_r^L is the radiation potential of the L^{th} motion. The unknown terms ϕ_d and ϕ_r^L are addressed next.

The diffraction term ϕ_d

The linear diffraction term and its boundary conditions can be expressed by the oscillatory function:

$$\phi_d(x,z,y) = \varphi_d(x,z)\ \exp(jky\sin\theta), \tag{7}$$

$$\frac{\partial\varphi_d}{\partial z} - \frac{\omega^2}{g}\varphi_d = 0\ \ (z = 0\ ), \tag{8}$$

$$\frac{\partial\varphi_d}{\partial z} = 0\ \ (z = -h), \tag{9}$$

$$\frac{\partial\varphi_d}{\partial n} = -\frac{\partial\varphi_i}{\partial n}\ \ \ (\text{on } S_0), \tag{10}$$

$$\lim_{x\to\infty}\left[\frac{\partial\varphi_d}{\partial x} \pm jk\cos\theta\ \varphi_d\right] = 0. \tag{11}$$

The boundary value problem here for diffraction potential is defined by the governing Laplace equation and then the boundary conditions are defined from Equation (8) to Equation (11), where n is the unit normal vector outward the body surface and S_0 is the wetted surface of the breakwater.

The radiation term ϕ_r^L

In the framework of the linear theory, the radiation term and its boundary conditions can be described by the following oscillatory radiation potentials:

$$\phi_r^L(x,z,y) = -j\omega A_r^L\ \varphi_r^L\ (x,z)\ \exp(jky\sin\theta), \tag{12}$$

$$\frac{\partial\varphi_r^L}{\partial z} - \frac{\omega^2}{g}\ \varphi_r^L = 0\ \ (z = 0), \tag{13}$$

$$\frac{\partial\varphi_r^L}{\partial z} = 0\ \ (z = -h), \tag{14}$$

$$\frac{\partial\varphi_r^L}{\partial z} = \delta_{1,L} - (x - x_0)\delta_{3,L} \qquad (z = -d\ , |x| \le a/2), \tag{15}$$

$$\frac{\partial\varphi_r^L}{\partial x} = \delta_{2,L} + (z - z_0)\delta_{3,L} \qquad (-d \le z \le 0\ \ , |x| = a/2), \tag{16}$$

$$\lim_{x\to\infty}\left[\frac{\partial\varphi_r^L}{\partial x} \pm jk\cos\theta\ \varphi_r^L\right] = 0, \tag{17}$$

where

$$\delta_{x,y} = \begin{cases} 1 & x = y \\ 0 & x \neq y \end{cases} \tag{18}$$

The amplitude of the L^{th} motion is denoted by A_r^L and (x_0, z_0) is the body centroid. Also, $\delta_{x,y}$ is known as Kronecker delta. The boundary value problem here for radiation potential is defined by the governing Laplace equation and then the boundary conditions are defined from Equation (13) to (17).

Hydrodynamic coefficients and wave forces

The wave force perpendicular to the incident wave is denoted as F_{w_u}, which is independent of y or time, and can be calculated from the incident and diffracted wave potentials as:

$$F_{w_u} = \rho j \omega \int_{S_0} (\varphi_d + \varphi_i)\, n_u \,\mathrm{d}s, \qquad (19)$$

in which n_u is the generalized inward normal to the structure in $x-z$ plane with $n_1 = n_z$, $n_2 = n_x$ and $n_3 = (z - z_0)n_x - (x - x_0)n_z$ with n_x and n_z being the unit inward normal to the surface of the body. Also, CF_u is the exciting force coefficient which is a non-dimensional form of F_{w_u} given by:

$$CF_u = \begin{cases} \dfrac{|F_{w_u}|}{\rho g a d A_i} & u = 1,2 \\ \dfrac{|F_{w_u}|}{0.5 \rho g a^2 d A_i} & u = 3 \end{cases} \qquad (20)$$

Transmission coefficient (T_w) is defined as the amplitude of the transmitted wave to that of the incident wave. Reflection coefficient (R_w) is defined as the amplitude of the reflected wave to that of the incident wave. Longuet-Higgins (1977) proposed horizontal drift force (F_d) in terms of the reflection coefficient as:

$$F_d = \left(\frac{E c_g}{c}\right)(1 + R_w^2 - T_w^2) = \left(\frac{2 E c_g}{c}\right) R_w^2, \quad (21)$$

where c_g is the wave group velocity, c is the phase velocity, $E = \frac{1}{2}\rho g {A_i}^2$ is the wave energy. The exciting force coefficients are calculated using Equation (20) and the transmission and reflection coefficients are evaluated using Equation (21). The far field method proposed by Newman et al. (1967), which is based on momentum conservation, is used for calculating steady drift. More details of this method could be found in Newman et al. (1967) and Lee and Newman (2005).

3. Results

The numerical panel method in ANSYS AQWA is used for carrying out the hydrodynamic analysis in frequency domain. In this method, the submerged part of the structure is divided into a finite number of panels on which the hydrodynamic pressures, added mass and damping coefficients of the body are calculated by the potential flow theory. More information on this method including formulation, boundary conditions and the discretization scheme could be found in Lee and Newman (2005). In this study, wave forces and diffraction analysis are evaluated using ANSYS AQWA diffraction analysis system, based on the linear wave theory.

For verification purposes, a typical rectangular FB in a domain of $h/d = 2$ and $a/2d = 1,3$ with zero angle of incidence ($\theta = 0$) is considered. Figure 2 shows the exciting force coefficients (CF_u) compared to the analytical studies of Black et al. (1971) and Zheng et al. (2004). Evidently, very good agreement is achieved.

The maximum element size in this numerical scheme is explicitly related to the maximum wave frequency considered in the diffraction analysis. For this purpose, after testing a number of maximum element size, the nearest value to the desired frequency range ($0 < f_i < 0.3\ Hz$) is chosen. Desired frequency range is calculated according to Equation (5) with respect to the desired wave number to cover a range of response, similar to previous studies. Also despite of the fact that CF_u is nondimensionlised with respect to A_i according to Equation (20), for evaluation purposes, throughout the present study it is assumed that $A_i = 1$ m.

General two-legged FBs

Figure 3 shows a general configuration of the two-legged rectangular FB. Cases of $\alpha = 0$ correspond to the Π type FBs and $\alpha = 90^0$ to the inverse T type. For analysis purpose, dimensionless parameters including a/h, h/d_1, e/f, a/f and α are considered, but not for the effect of breakwater weight, similar to previous studies like Zheng et al. (2004). It must be pointed

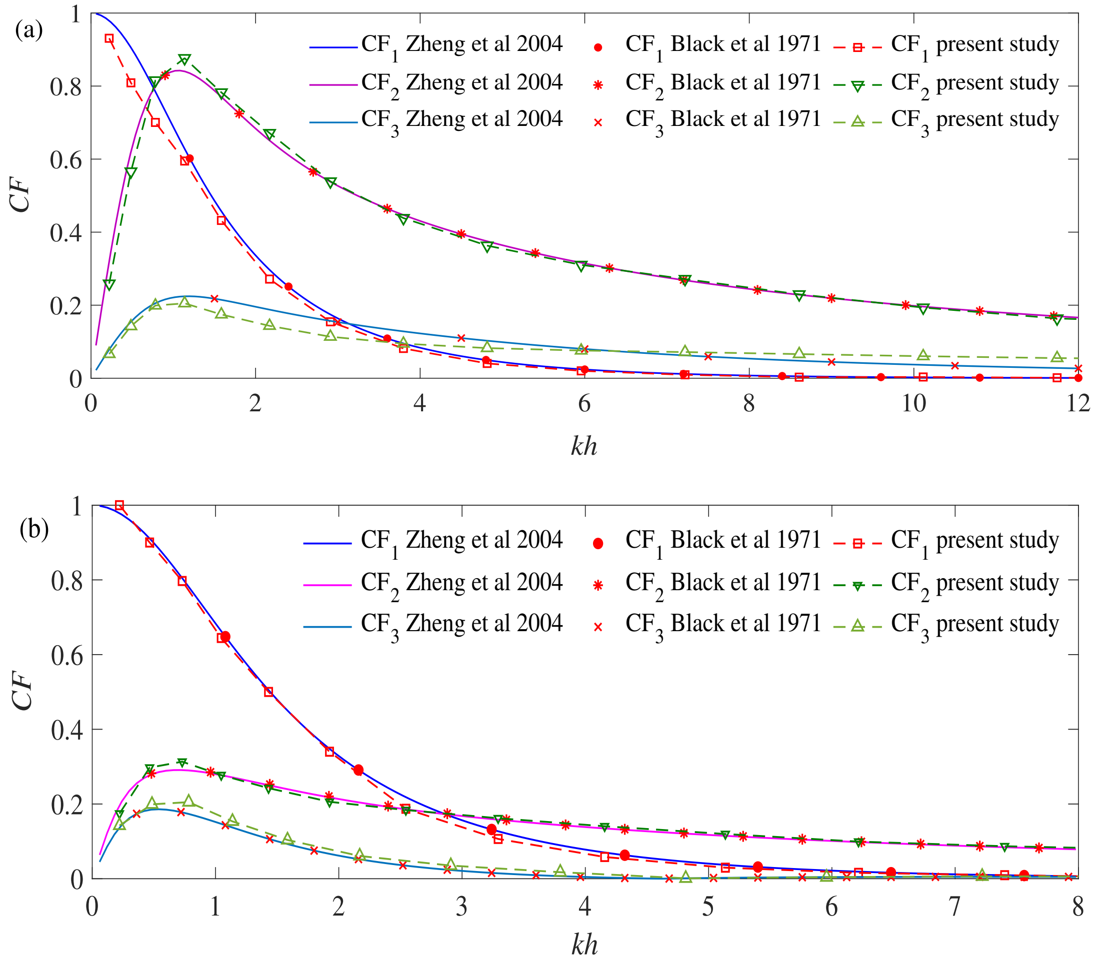

Figure 2: Result comparison of the present study on exciting force coefficients CF_u on FB of (a) $a/2d = 1$ and (b) $a/2d = 3$ with analytical results of Zheng et al. (2004) and Black et al. (1971) for heave ($u = 1$), sway ($u = 2$) and roll ($u = 3$) motions/directions ($h/d = 2, \theta = 0$)

out that given the same material, altering any of those dimensionless parameters will result in weight change in reality. Adjusting those parameters without the weight means that the weight changing is automatically accounted for in the final result. Although this could be helpful for illustration purpose, the true hydrodynamic effect of those parameters cannot be isolated. Since weight, hence the material selection, is usually considered as one of the most important factors in breakwater design, its effect must be considered separately. To limit the scope of the current study, the analyses here are for constant weight, i.e. the cross sectional area below the water level is constant for all the cases considered. Also $d_2 = d_1 - f\cos(\alpha) - e\sin(\alpha)$ is a dependent parameter on d_1 and so is not considered as a main parameter in this study.

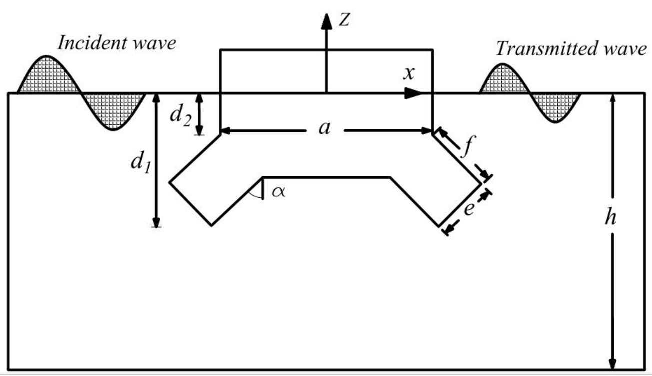

Figure 3: Basic configuration and coordinate system for rectangular two-legged FB

In analyzing two-legged FBs, it should be noted that flow separation is likely to occur in

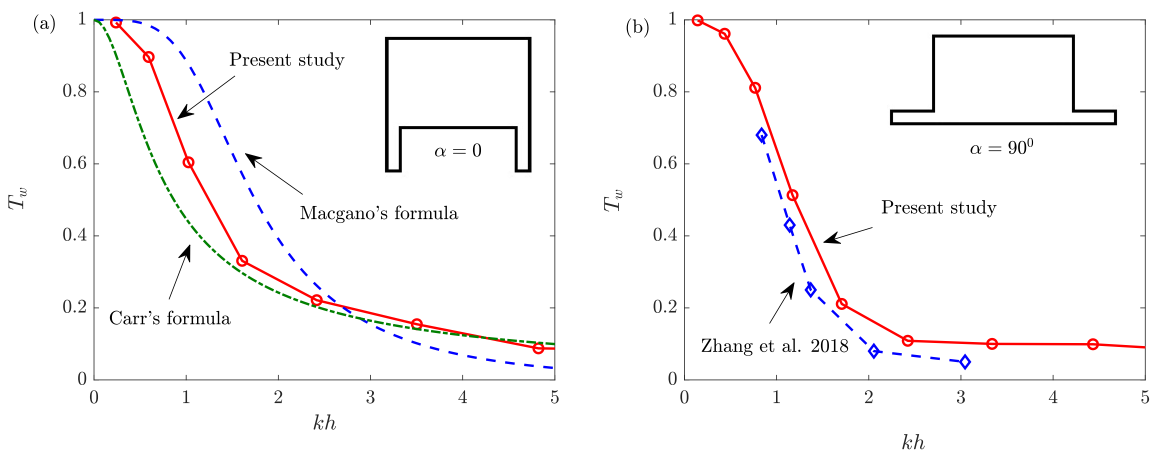

Figure 4: Transmission coefficient comparison of (a) $\alpha = 0$ of the present study ($a/h = 1, h/d_1 = 2, e/f = 1, a/f = 4$) compared with Carr's formula (Carr, 1951) and Macgano's formula (Macagno, 1954) and (b) $\alpha = 90^0$ of present study ($a/h = 0.4, h/d_1 = 3, e/f = 0.25, a/f = 2$) compared with the experimental results of Zhang et al. (2018) for $e/f \approx 0$.

real-world applications and therefore boundary layer effect becomes important. Here, this effect is not taken into consideration following a number of studies (such as Gesraha (2006), Cho (2016) and Deng et al. (2019b)) at similar working conditions. Moreover, our results are validated against previous studies in two cases of legged-FBs of $\alpha = 0$ and $\alpha = 90^0$. For $\alpha = 0$, Kolahdoozan et al. (2017) showed that Carr's transmission coefficient formula, which was firstly proposed by Carr (1951), matched satisfactorily with the experimental data for intermediate waters, and that Macgano's formula proposed by Macagno (1954) could be used for deep waters. In Figure 4 (a), both formulas are compared to the present results, which demonstrates reasonable agreement. Comparison with the experimental results of Zhang et al. (2018) is also presented in Figure 4 (b) for $\alpha = 90^0$, which also suggests acceptable agreement in spite of the slight difference in the e/f values. It should be mentioned that the condition $e/f = 0$ in Zhang et al. (2018) could not be adopted for the current study based on the limitations of the panel method, and therefore $e/f = 0.25$ is used for this figure.

Leg angle (α) effect

To investigate the leg angle effect, a FB in a domain of $a/h = 1$, $h/d_1 = 2$, $e/f = 1$, and $a/f = 4$ is considered. Also α is assumed to be dispensed in six equal increments from zero giving $\alpha = 0, 15^0, 30^0, 45^0, 60^0, 75^0, 90^0$. The center of rotation for all breakwaters is at $(0, z_0)$ in which z_0 is considered to be the center of buoyancy.

Figure 5 illustrates the variation of CF_u with respect to kh in three degrees of freedom. Apparently, increasing α results in decreasing CF_1 at low kh values before a large increment for $\alpha \geq 45^0$. On the contrary, CF_2 increases at low kh but decreases at $kh > 1$ for all α. Maximum CF_2 increases with increasing α. Also increasing α results in moment (CF_3) increment for $\alpha \geq 45^0$ but decrement for $\alpha < 45^0$.

Figure 6 displays the effect of the transmission and reflection coefficients on α, according to Equation 21. Firstly, it is obvious that the effect of α is weak, in line with the fact that cross sectional areas are equal in all the cases. Secondly, increasing α leads to decreasing T_w and increasing R_w for water depth, which means that in general, increasing the leg angle could enhance breakwater's efficiency in linear waves. Also, the inverse T type and the Π type FBs are the most and the least efficient two-legged FBs in this respect. Furthermore, considering the fact that for $kh > 5$ the reflection coefficients for all cases go to unity approximately, using different configurations in deep water or very high wave numbers would result in the same transmission coefficient.

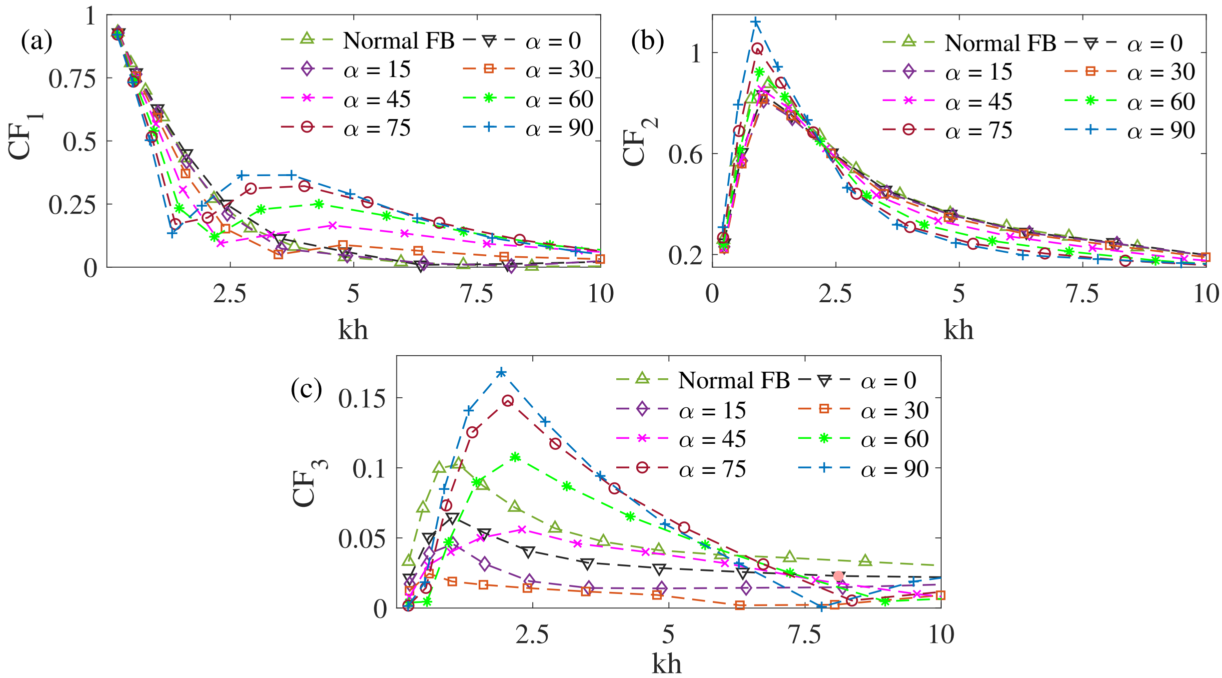

Figure 5: Leg angle effect on exciting force coefficients. $(a/h = 1, h/d_1 = 2, e/f = 1, a/f = 4)$

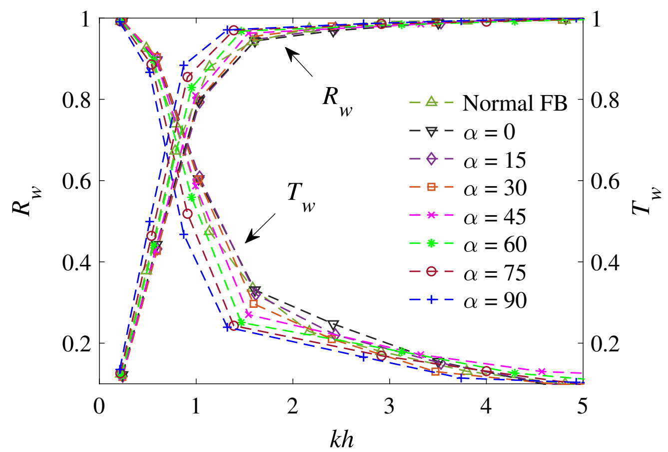

Figure 6: Leg angle effect on transmission and reflection coefficients. $(a/h = 1, h/d_1 = 2, e/f = 1, a/f = 4)$

Leg size (e/f) *effect*

Here we consider the dimensionless parameter e/f, in which e denotes the leg width and f its length. Assuming $d_2 > 0$ for all the cases, eight different values of e/f between 0.6 and 1.4 are considered to be compared to $e/f = 1$ in the previous section. Also, α is fixed at 45^0. Other α should demonstrate similar trend since a/f is held constant. Figure 7 shows the exciting force coefficients varying upon the leg size. CF_1 shows little difference for all the cases for $kh < 2.45$. However, after that, increasing e/f causes increasing vertical exciting force. CF_2 on the other hand shows a very opposite trend. For $kh < 2.45$, all the cases share identical horizontal exciting force, but for $kh > 2.45$, increasing e/f results in diminishing CF_2. Moreover, according to Figure 7 (c), maximum exciting moment increases as e/f. The effect of e/f on CF_3 is more pronounced for $kh > 2.45$, apparently as a result of the opposite behaviour of CF_1 and CF_2.

Figure 8 shows the variation of transmission and reflection coefficients on e/f. It is clear that the effect is almost negligible. Note that the weight effect is eliminated. The effect of width is also removed by considering a/f constant in all cases. As a conclusion one might understand that e/f has almost no effect on transmission and reflection coefficients. However it takes effects on exciting force coefficients as shown in Figure 7 which is vital in mooring design and configuration.

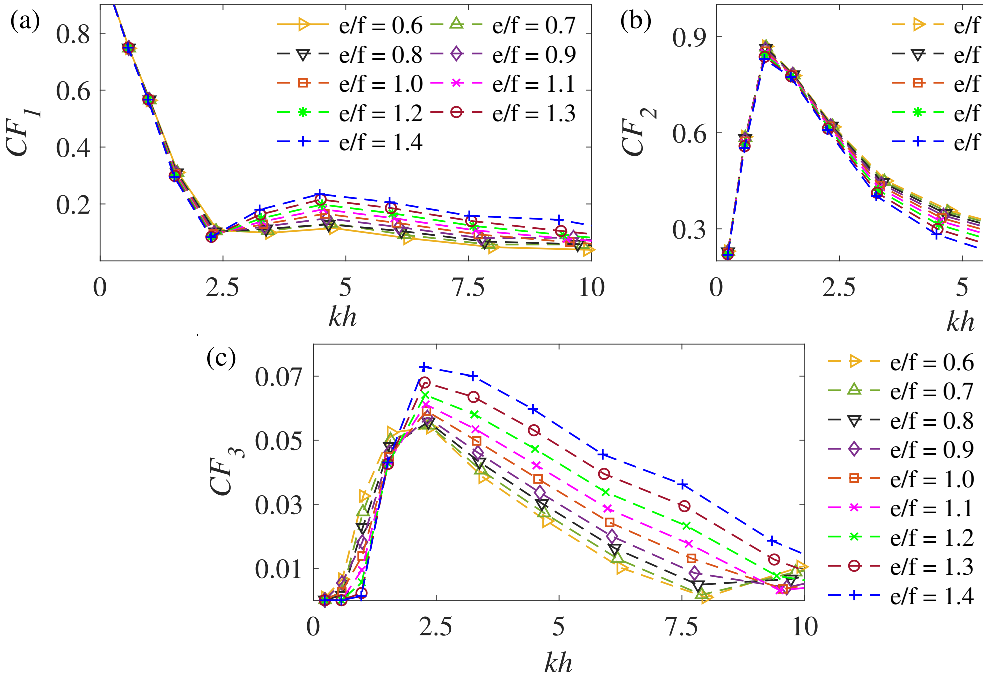

Figure 7: Leg size effect on exciting force coefficients. $(a/h = 1, h/d_1 = 2, \alpha = 45^0, a/f = 4)$

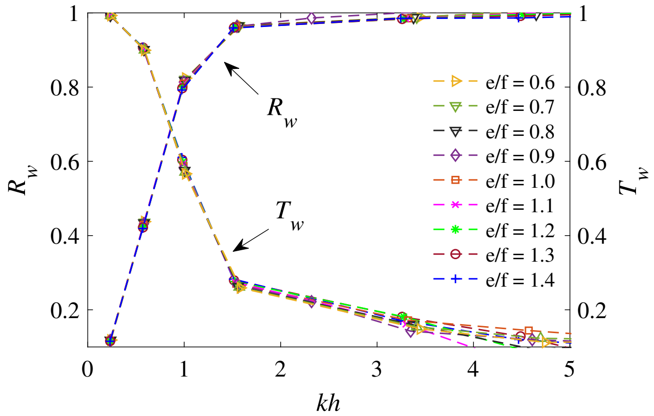

Figure 8: Leg size effect on transmission and reflection coefficients. $(a/h = 1, h/d_1 = 2, \alpha = 45^0, a/f = 4)$

4. Discussion

It is suggested in the previous section that α has considerable effect on T_w, R_w and CF_u, and hence the efficiency of the FB. The ratio e/f, however, takes a weak effect on the two coefficients but some upshot on CF_u. In order to have better understanding of the hydrodynamic performance of the breakwaters, Figure 9 illustrates the projection area (in length) of the FB along z (A_{rz}) and x (A_{rx}) directions. A_r is normalised by the square root of the cross sectional area. Apparently increasing α, holding constant $e/f = 1$, leads to monotonic decrease of A_{rz} but A_{rx} behaves in a parabolic manner and and peaks at $\alpha \approx 45^0$. On the other hand, increasing e/f in constant $\alpha = 45^0$ leads to decreasing A_{rx} and A_{rz}.

Figure 5 which shows the α effect on CF_u reveals some physical properties of two-legged FBs. According to Figure 5 (a), CF_1 in normal rectangular FB and $\alpha \leq 15^0$ continuously decreases over the tested kh range. However, for $\alpha = 30^0$ a hump appears at $kh_{hump} \approx 3.5$. This should be because of the vertical force component on the legs. So as α increases this vertical component, $F_u \cos(\alpha)$, increases and reaches its maximum at $\alpha = 90^0$. Also as α increases, the average draft of the projected area along the z direction, A_{rz}, decreases, which promotes the hump in CF_1 as well. The main physical reason for this hump to occur is that the wave energy (summation of the diffraction and incident waves) gets weaker as the average draft increases. Therefore having lower draft will result in higher pressure distributions which leads to larger CF_1. Furthermore, kh_{hump} decreases with increasing α. It infers that low frequencies or large wavelengths of incident waves induce stronger vertical component of the exciting force. This is attributing to the fact that for high frequency waves in which multiple crests and troughs impact on a certain surface, the total vertical pressure component would be close to zero. Nevertheless for low frequencies, especially when wavelength is less than the projected length, the net vertical force will be larger. Here as the height of the water is different in each case, kh_{hump} is diverse.

The horizontal force coefficient in Figure 5 (b) can be considered as two parts, $kh < 2.4$ and $kh > 2.4$. As α increases, horizontal force CF_2 increases accordingly in the first part, but decreases in the second part. It means that in low frequencies of the incident wave, high α values lead to larger CF_2, but opposite for high frequencies. As a matter of fact, according to Figure 9, increasing α coincides with decreasing A_{rz}, hence weaker horizontal force impact for $kh > 2.4$. For $kh < 2.4$ low frequency waves induce larger forces (globally) on the body due to asymmetric pressure distribution. Also, for $0^0 \leq \alpha \leq 75^0$ there are two projected surfaces along z direction on each side of the leg, which takes opposing horizontal force components, one in $(+x)$ direction changing with $\cos(\alpha)$ and one in $(-x)$ direction changing with $\sin(\alpha)$. So for $kh < 2.4$, CF_2 increases with α and finally the term associated with $\sin\alpha$ vanishes as $\alpha = 90^0$. This leads to higher CF_2 magnitude as shown in Figure 5 (b). Figure 5 (c) suggests that for small wave number range $kh \lesssim 7.5$, the the structure becomes unstable for large α, i.e. for $\alpha = 90^0$ the maximum exciting moment is 50% larger than that in conventional FBs.

In Figure 7 (a) similar humps start at $kh_{hump} \approx 2.3$. For smaller kh, CF_1 in all the cases are nearly identical. For larger kh, CF_1 increases with e/f. It may also be explained by the total wave energy distribution. Although case $e/f = 1.4$ has the lowest A_{rx} (very weak difference), the vertical force is larger for $kh > 2.3$. This is because in this case draft (d) is much lower comparing to other cases and therefore the induced pressure is much stronger. Recalling the fact that most of the wave energy is on the water surface, as draft increases, less energy would be induced to the body in z direction. In addition, increasing e/f results in decreased d because of the constant weight. Consequently, for other cases like $e/f = 0.6$, in spite of larger A_{rz}, the draft is high but the wave energy exerts on the body in the z direction is not as large as in $e/f = 1.4$.

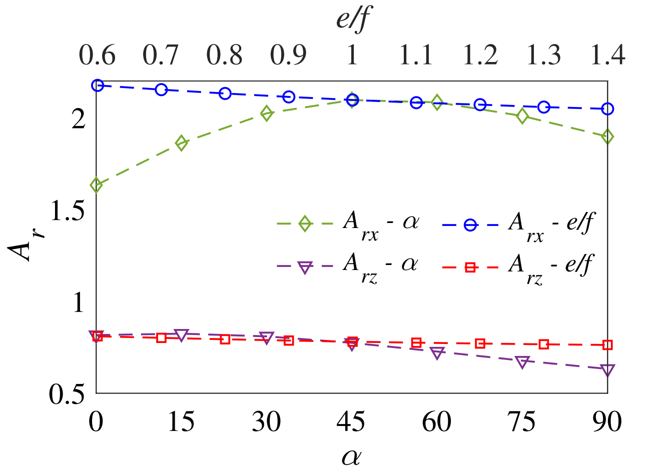

Figure 9: Dimensionless projection area (in length) along x and z directions for e/f and α series presented is section 3

Figure 7 (b) shows that all cases share similar maximum horizontal exciting force coefficient. This is due to the fixed α leading to analogous force decomposition in x and z direction. For large kh, CF_2 diminishes as e/f increases because of the symmetric pressure distribution on the body in high frequency waves. However higher e/f values lower CF_2, which is a direct consequence of increasing projected area along z direction with decreasing e/f. Another observation is that increasing e/f vanishes CF_2 at smaller kh. In practice this means larger e/f do not result in higher maximum horizontal exciting forces. This however, gives rise to higher vertical force according to Figure 7 (a). Figure 7 (c) shows exciting moments for different e/f. The trajectories are a direct result of horizontal and vertical forces, which are discussed above.

Figure 6 and Figure 8 show the behaviour of T_w and R_w, respectively. Obviously, leg size has little effect on the two coefficients. On the other hand, leg angle effect is considerable. Practically, it suggests that efficiency increases with α for given leg length and breakwater weight. In

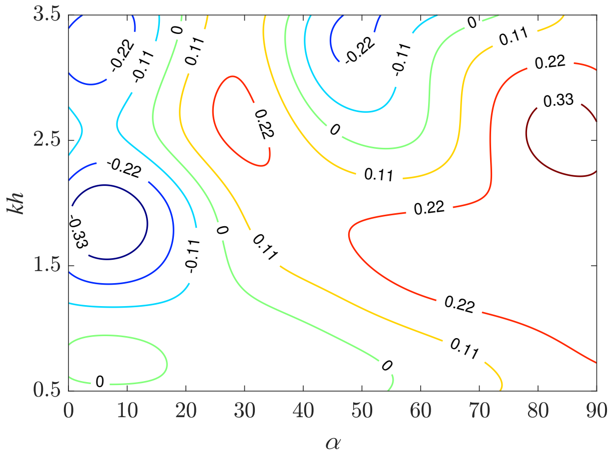

Figure 10: Dependence of the leg angle effect on the efficiency (based on T_w) of the breakwater compared to normal rectangular FB ($a/h = 1, h/d_1 = 2, e/f = 1, a/f = 4$).

order to illustrate leg angle effect in various kh conditions, Figure 10 is shown, which represents the change in T_w compared to the normal rectangular FB of the same weight. It shows that at $\alpha = 90^0$, efficiency can increase by $\approx 30\%$ for $kh = 1.5$, which is significant. On the contrary, $\alpha = 0$ experiences $\approx 30\%$ efficiency drop at $kh = 2$. In general, for all kh values, efficiency is largely proportional to α. Accordingly one may speculate that increasing α beyond 90^0 could have an even better efficiency gain. However, since at some α in that range, the legs will break through the free surface, the variation and behaviour of transmission and reflection coefficients will be much more complicated, which deserves a comprehensive study. Other parameters which can affect the efficiency of the breakwater are $a/h, h/d_1$. These parameters have been studied extensively for different types of breakwaters including floating and submerged (Dong et al., 2008; Peña et al., 2011; Masoudi and Zeraatgar, 2016; Masoudi and Gan, 2020). In these studies, the width of the breakwater is reported to be the governing parameter for transmission and reflection coefficients. In the context of the present study, increasing the draught of the breakwater for constant weight might lead to a smaller width and in that case it will result in a lower efficiency.

The main factor to determine the behaviour of T_w and R_w in different wave frequencies is the diffraction wave formation on the FBs. Figure 11 (a,b) show the dimensionless diffraction wave amplitude (A_d/A_i) alongside the body in x axis for phase angle $\pi/2$. It can be noticed that e/f has weak effect on the wave amplitude, whilst large α induces large diffraction waves on the body, which lower the transmission coefficient and therefore increase the efficiency. Figure 11 (c,d) also show the dimensionless maximum diffraction wave amplitude for different incident wave frequencies (f_i) separating the α and the e/f effects for zero phase angle. Both figures show that $A_{d_{max}}/A_i$ converges to ≈ 1.2 at high frequency. The convergence of $A_{d_{max}}/A_i$ was also observed in Masoudi and Gan (2020) for submerged breakwaters and shows a minimum transmission coefficient almost zero in high incident wave frequencies ($f_i > 0.3$ in this case). Comparing (c) and (d) reveals that larger α leads to higher $A_{d_{max}}/A_i$ and this is the main reason for diminishing T_w in Figure 6. The weak dependence on e/f is in line with the small T_w variation in Figure 8.

Furthermore, the hump observed in CF_1 in Figure 5 and Figure 7 coincides with the trough in $A_{d_{max}}/A_i$. It can be concluded that the hump in the exciting forces (which are integrals of incident and diffraction wave potentials over the projection length according to Equation 20) is directly connected to the hump in diffraction wave amplitude. There is almost no hump observed in $\alpha < 30^0$ and it well agrees with Figure 5 (a). In $\alpha = 30^0$ a small change in $A_{d_{max}}/A_i$ appears in $f_i \approx 0.06-0.15$ and as α increases, this change becomes larger. Globally, an increase in diffraction wave amplitude can be observed which is responsible for lower T_w in high α. Locally, a hump which starts from f_{hump} in all the α cases can be considered as the main reason for the hump in CF_1.

The reason for the trough and crest emerging in $A_{d_{max}}/A_i$ trend at $f_i \approx 0.06-0.15$ is most likely related to the linear intrinsic essence of diffraction problem. As a linear problem the total velocity potential (ϕ_t) can be divided into single potential components (ϕ_d, ${\phi_r}^L$ and ϕ_i) as shown in Equation (6). The diffraction potential itself (ϕ_d) has a similar behaviour. In case of a two-legged FB, the total diffraction potential can be assumed to be

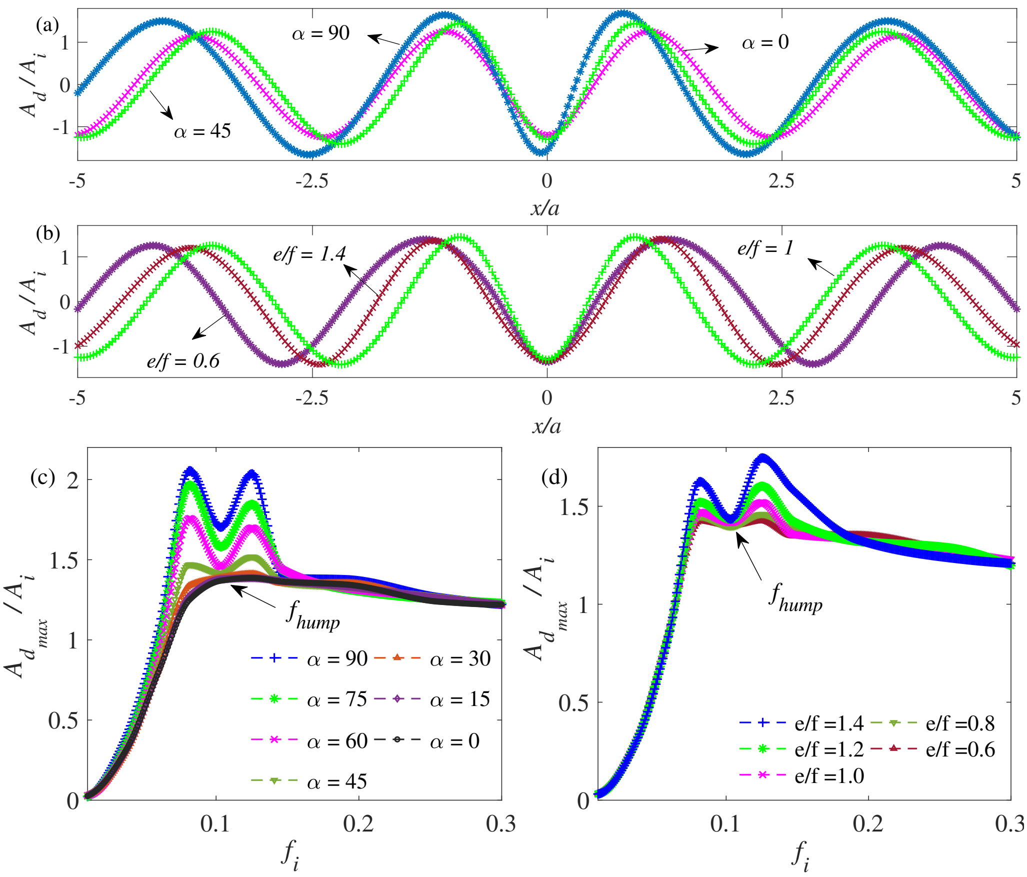

Figure 11: (a,b) Dimensionless diffraction wave amplitude A_d/A_i. (a) ($a/h = 1, h/d_1 = 2,\ a/f = 4,\ e/f = 1$ and $\alpha = 0,\ 45^0,\ 90^0$) and (b) ($a/h = 1,\ h/d_1 = 2,\ \alpha = 45^0,\ a/f = 4$ and $e/f = 0.6, 1, 1.4$) all in $f_i = 0.11\ Hz$ and phase angle of $\pi/2$; (c,d) Dimensionless maximum diffraction wave amplitude $A_{d_{max}}/A_i$ on two-legged FBs of (c) ($a/h = 1,\ h/d_1 = 2,\ a/f = 4,\ e/f = 1$ and $\alpha = 0, 15^0, 30^0, 45^0, 60^0, 75^0, 90^0$) and (d) ($a/h = 1,\ h/d_1 = 2,\ a/f = 4, \alpha = 45^0$ and $e/f = 1.4 - 1.2 - 1.0 - 0.8 - 0.6$) all in zero phase angle.

composed of the potential induced by each leg and the potential induced by the mid-body. So there are three potential terms and three diffraction wave amplitudes. The amplitude that is shown in Figure 11 is a summation due to the interaction of those amplitudes and that is why it does not follow the logarithmic normal trend of $A_{d_{max}}/A_i$. More investigation in this field is needed to further clarify such phenomena and their effects on the hydrodynamic performance of FBs.

5. Conclusions

In this study two-legged FBs with rectangular cross section in finite water depth in regular waves are studied for further implementation. For a constant total cross sectional area, leg angle and leg size as most important parameters are analysed and their hydrodynamic effects are quantified by a numerical panel method. The following conclusions can be drawn:

- The leg size parameter e/f has little effect on diffraction wave amplitude and so the transmission coefficient. On the other hand, the leg angle α has a considerable effect.

- The diffraction wave amplitude plays an important role in breakwater's hydrodynamic performance in sinusoidal waves and configurations that produce larger diffraction waves are more efficient. Diffraction wave amplitude however depends on many factors, but this study shows that in two-legged breakwaters, leg angle α takes more effect than leg length.

- A hump in vertical exciting force for moderate dimensionless wave numbers kh may happen due to the force (CF_u) decomposition of the legs and higher diffraction wave amplitudes. This hump mostly depends on leg angle (α) rather than leg length (e/f) and it occurs in lower kh values for larger leg angles.

- Two-legged breakwaters can be better alternatives to conventional rectangular FBs. It is suggested that they can increase the efficiency of the breakwater in the same weight up to 35%. Among two-legged breakwaters, the inverse T type FB ($\alpha = 90^0$) has the best and the Π ($\alpha = 0$) type breakwater has the least efficiency in a vast range of incident wave frequencies.

References

Abul-Azm, A., Gesraha, M., 2000. Approximation to the hydrodynamics of floating pontoons under oblique waves. Ocean Engineering 27, 365–384.

Bai, K.J., 1975. Diffraction of oblique waves by an infinite cylinder. Journal of Fluid Mechanics 68, 513–535.

Black, J.L., Mei, C.C., Bray, M.C.G., 1971. Radiation and scattering of water waves by rigid bodies. Journal of Fluid Mechanics 46, 151–164.

Carr, J.H., 1951. Mobile breakwaters. Coastal Engineering Proceedings , 25–25.

Chen, B., Ning, D., Liu, C., Greated, C.A., Kang, H., 2016. Wave energy extraction by horizontal floating cylinders perpendicular to wave propagation. Ocean Engineering 121, 112–122.

Cho, I.H., 2016. Transmission coefficients of a floating rectangular breakwater with porous side plates. International journal of naval architecture and ocean engineering 8, 53–65.

Deng, Z., Ren, X., Wang, L., Wang, P., 2019a. Hydrodynamic performance of a novel oscillating-water-column breakwater with a horizontal bottom-plate: Experimental and numerical study. Ocean Engineering 187, 106174.

Deng, Z., Wang, L., Zhao, X., Huang, Z., 2019b. Hydrodynamic performance of a t-shaped floating breakwater. Applied Ocean Research 82, 325–336.

Dong, G., Zheng, Y., Li, Y., Teng, B., Guan, C., Lin, D., 2008. Experiments on wave transmission coefficients of floating breakwaters. Ocean Engineering 35, 931–938.

Garrison, C., 1984. Interaction of oblique waves with an infinite cylinder. Applied Ocean Research 6, 4–15.

Gesraha, M.R., 2006. Analysis of π shaped floating breakwater in oblique waves: I. impervious rigid wave boards. Applied Ocean Research 28, 327 – 338.

Ghafari, H., Dardel, M., 2018. Parametric study of catenary mooring system on the dynamic response of the semi-submersible platform. Ocean Engineering 153, 319–332.

Günaydın, K., Kabdaşlı, M., 2007. Investigation of π-type breakwaters performance under regular and irregular waves. Ocean Engineering 34, 1028 – 1043.

He, F., Zhang, H., Zhao, J., Zheng, S., Iglesias, G., 2019. Hydrodynamic performance of a pile-supported owc breakwater: An analytical study. Applied Ocean Research 88, 326 – 340.

Hur, D.S., Mizutani, N., 2003. Numerical estimation of the wave forces acting on a three-dimensional body on submerged breakwater. Coastal Engineering 47, 329–345.

Kolahdoozan, M., Bali, M., Rezaee, M., Moeini, M.H., 2017. Wave-transmission prediction of π-type floating breakwaters in intermediate waters. Journal of Coastal Research 33, 1460–1466.

Lau, S., Ji, Z., Ng, C., 1990. Dynamics of an elastically moored floating body by the three-dimensional infinite element method. Ocean engineering 17, 499–516.

Lee, C.H., Newman, J., 2005. Computation of wave effects using the panel method. WIT Transactions on State-of-the-art in Science and Engineering 18.

Lee, J.F., 1995. On the heave radiation of a rectangular structure. Ocean Engineering 22, 19–34.

Liu, Z., Wang, Y., Wang, W., Hua, X., 2019. Numerical modeling and optimization of a winged box-type floating breakwater by smoothed particle hydrodynamics. Ocean Engineering 188, 106246.

Longuet-Higgins, M.S., 1977. The mean forces exerted by waves on floating or submerged bodies with applications to sand bars and wave power machines. Proceedings of the Royal Society of London. A. Mathematical and Physical Sciences 352, 463–480.

Macagno, E.O., 1954. Houle dans un canal présentant un passage en charge. La Houille Blanche , 10–37.

MacCamy, R., Fuchs, R.A., 1954. Wave forces on piles: a diffraction theory. 69, US Beach Erosion Board.

Masoudi, E., 2019. Hydrodynamic characteristics of inverse t-type floating breakwaters. International Journal of Maritime Technology 11, 13–20.

Masoudi, E., Gan, L., 2020. Diffraction waves on large aspect ratio rectangular submerged breakwaters. Ocean Engineering 209, 107–474.

Masoudi, E., Zeraatgar, H., 2016. Application of method of separation of variables for analyzing floating breakwater. Journal of Marine Engineering 11, 61–73.

Michailides, C., Angelides, D.C., 2012. Modeling of energy extraction and behavior of a flexible floating breakwater. Applied Ocean Research 35, 77–94.

Newman, J.N., et al., 1967. The drift force and moment on ships in waves. Journal of ship research 11, 51–60.

Peña, E., Ferreras, J., Sanchez-Tembleque, F., 2011. Experimental study on wave transmission coefficient, mooring lines and module connector forces with different designs of floating breakwaters. Ocean Engineering 38, 1150–1160.

Shen, Y., Zheng, Y., You, Y., 2005. On the radiation and diffraction of linear water waves by a rectangular structure over a sill. part i. infinite domain of finite water depth. Ocean Engineering 32, 1073–1097.

Ursell, F., 1949. On the heaving motion of a circular cylinder on the surface of a fluid. The Quarterly Journal of Mechanics and Applied Mathematics 2, 218–231.

Wang, G., Drimer, N., Goldfeld, Y., 2020. Modular floating structures (mfs) for offshore dwelling a hydrodynamic analysis in the frequency domain. Ocean Engineering 216, 107996.

Wu, G., Taylor, R.E., 1995. Time stepping solutions of the two-dimensional nonlinear wave radiation problem. Ocean Engineering 22, 785–798.

Xu, X., Song, X., Zhang, X., Yuan, Z., 2019. On wave diffraction of two-dimensional moonpools in a two-layer fluid with finite depth. Ocean Engineering 173, 571 – 586.

Yamamoto, T., Yoshida, A., Ijima, T., 1980. Dynamics of elastically moored floating objects. Applied ocean research 2, 85–92.

Zhan, J.m., Chen, X.b., Gong, Y.j., Hu, W.q., 2017. Numerical investigation of the interaction between an inverse t-type fixed/floating breakwater and regular/irregular waves. Ocean engineering 137, 110–119.

Zhang, X.s., Ma, S., Duan, W.y., 2018. A new l type floating breakwater derived from vortex dissipation simulation. Ocean Engineering 164, 455–464.

Zheng, Y., You, Y., Shen, Y., 2004. On the radiation and diffraction of water waves by a rectangular buoy. Ocean engineering 31, 1063–1082.